JGR Atmospheres

RESEARCH ARTICLE
10.1029/2024JD042158

Decoding the Relationship Between Cloud Electrification, Downdrafts, and Surface Ozone in the Amazon Basin

Gabriela R. Unfer[1,2,3], Luiz A. T. Machado[2,4], Rachel I. Albrecht[5], Micael A. Cecchini[5], Hartwig Harder[6], Flávio C. Magina[3], Mira L. Pöhlker[1,7], Ulrich Pöschl[2], Jordi Vilà-Guerau de Arellano[8], Earle R. Williams[9], Stefan Wolff[2], and Christopher Pöhlker[2]

[1]Atmospheric Microphysics Department, Leibniz Institute for Tropospheric Research, Leipzig, Germany, [2]Multiphase Chemistry Department, Max Planck Institute for Chemistry, Mainz, Germany, [3]Center for Weather Forecasting and Climate Research, National Institute for Space Research, Cachoeira Paulista, Brazil, [4]Institute of Physics, University of São Paulo, São Paulo, Brazil, [5]Institute of Astronomy, Geophysics and Atmospheric Sciences, University of São Paulo, São Paulo, Brazil, [6]Atmospheric Chemistry Department, Max Planck Institute for Chemistry, Mainz, Germany, [7]Faculty of Physics and Earth Sciences, Leipzig Institute for Meteorology, Leipzig University, Leipzig, Germany, [8]Meteorology and Air Quality Section, Wageningen University Research, Wageningen, The Netherlands, [9]Massachusetts Institute of Technology, Cambridge, MA, USA

Key Points:

- Surface ozone level is affected by both downdrafts and cloud electrification, but at different ratios depending on their magnitudes
- The role of cloud electric field in increasing ozone surpasses that of downdrafts at higher field strengths
- A parameterization to estimate surface ozone during storms is introduced, accounting for the impact of cloud electrification and downdrafts

Supporting Information:

Supporting Information may be found in the online version of this article.

Correspondence to:

G. R. Unfer and L. A. T. Machado,
unfer@tropos.de;
l.machado@mpic.de

Citation:

Unfer, G. R., Machado, L. A. T., Albrecht, R. I., Cecchini, M. A., Harder, H., Magina, F. C., et al. (2025). Decoding the relationship between cloud electrification, downdrafts, and surface ozone in the Amazon Basin. *Journal of Geophysical Research: Atmospheres*, *130*, e2024JD042158. https://doi.org/10.1029/2024JD042158

Received 9 AUG 2024
Accepted 26 JAN 2025

Author Contributions:

Conceptualization: Gabriela R. Unfer, Luiz A. T. Machado
Data curation: Micael A. Cecchini, Flávio C. Magina, Stefan Wolff
Formal analysis: Gabriela R. Unfer
Funding acquisition: Gabriela R. Unfer, Luiz A. T. Machado
Investigation: Gabriela R. Unfer, Luiz A. T. Machado
Methodology: Gabriela R. Unfer, Luiz A. T. Machado
Project administration: Luiz A. T. Machado, Christopher Pöhlker
Supervision: Luiz A. T. Machado
Validation: Gabriela R. Unfer

Abstract The relationship between the electric field of storms and surface ozone (O_3) levels in the Amazon Tall Tower Observatory (ATTO) region was investigated. Our findings reveal that surface ozone concentrations increase with the rise in the absolute electric field ($|E_z|$) of clouds. This phenomenon is linked to the amplification of downdraft magnitudes, which are similarly associated with the $|E_z|$. Detailed analysis also indicated that stronger downdrafts correlate with higher surface ozone levels. Consequently, the $|E_z|$-downdrafts-O_3 interaction forms a coupled system, influenced by the strength of convective clouds. Notably, a more significant effect is observed when the $|E_z|$ surpasses the threshold of lightning activity, leading to an increment of up to 5 ppb_v in surface O_3. This increment was shown to be independent of downdraft intensity or cloud height, relating solely to the impact of electrical activity. Based on the observational data, a novel parameterization was developed to predict surface ozone concentrations during storms, effectively incorporating the proportional impact of cloud electrification and downdrafts. This phenomenological model provides a robust tool for understanding and forecasting ozone dynamics in storm events in the Amazon rainforest, highlighting the intricate interplay between cloud electricity, downdrafts, and air chemistry in tropical convective storms.

Plain Language Summary Cloud electrification is associated with complex processes that can produce ozone in the atmosphere. During storms, the combination of this electrification with air motion can modulate ozone concentrations near the surface. Therefore, we tested our hypothesis that surface ozone changes are correlated with clouds' electric field. The electric field of a storm measures how electrically charged the cloud is. We studied this relationship in a remote area of central Amazonia, at the Amazon Tall Tower Observatory (ATTO). The results confirm our hypothesis in the sense that surface ozone levels rise with increasing electrification of clouds. We disentangled the causes and effects: surface ozone increases due to the increased downward transport of tropospheric air which, in turn, is driven by the invigoration of thunderstorms, typically associated with an enhanced electric field. Beyond the circulation-driven ozone enhancement, we also found an additional ozone increment for strong electric fields that were associated with the presence of lightning activity. We also developed a model to predict surface ozone levels during storms, which successfully includes the balanced impact of cloud electrification and downdrafts. Overall, our study shows how thunderstorms, downdrafts, and electrical activity can work in different ways to affect surface ozone in the Amazon.

1. Introduction

Although vital in the stratosphere for filtering ultraviolet radiation, ozone (O_3) acts as a greenhouse gas in the troposphere and as a harmful air pollutant at surface levels. Conversely, O_3 in the presence of water vapor is a precursor of hydroxyl radical (OH) (McGrath & Norrish, 1958), a key tropospheric oxidant that controls the concentration of toxic pollutants (Lelieveld et al., 2004; Logan et al., 1981; Patra et al., 2014). Ozone then plays an ambivalent role at the surface, being an injurious pollutant when at high levels while also helping clean the atmosphere. Nitrogen oxides (NO_x) are an important precursor of O_3, coming from anthropogenic or natural

Visualization: Gabriela R. Unfer
Writing – original draft: Gabriela R. Unfer
Writing – review & editing: Gabriela R. Unfer, Luiz A. T. Machado, Rachel I. Albrecht, Micael A. Cecchini, Hartwig Harder, Flávio C. Magina, Mira L. Pöhlker, Ulrich Pöschl, Jordi Vilà-Guerau de Arellano, Earle R. Williams, Stefan Wolff, Christopher Pöhlker

sources (Grewe et al., 2012). Global biomass burning, for instance, is estimated to produce 14.65 ± 1.60 Tg NO_x $year^{-1}$ (Bray et al., 2021), while global lightning-NO_x (LNO_x) is estimated to produce about 5 ± 3 Tg of N $year^{-1}$ (Schumann & Huntrieser, 2007), a considerable amount. In the middle and upper tropical troposphere, LNO_x is the major precursor of O_3 (Bucsela et al., 2010; Finney et al., 2016; Martin et al., 2000). Meteorological parameters, such as temperature, humidity, and wind speed/direction can influence surface O_3 concentrations (Nguyen et al., 2022). However, O_3 levels are also affected by anthropogenic emissions and changes in greenhouse gas concentrations, which leads to unclear future O_3 trends in global warming scenarios (Karagodin-Doyennel et al., 2023), although the frequency of thunderstorms can be boosted, leading to more LNO_x and further O_3 (Lu et al., 2019; Sinha & Toumi, 1997; Toumi et al., 1996; Zeng et al., 2008). Romps et al. (2014) estimate an increase of 12% ± 5% per °C in lightning strikes in the United States, while Pinto Junior and Pinto (2020) show an increase of 35% per °C in lightning flashes in Rio de Janeiro. Other studies, though, demonstrated that the parameterizations chosen can vary the future trends of lightning, also showing a decrease in its activity (Clark et al., 2017; Finney et al., 2018). Thus, understanding ozone concentration variability is particularly important.

The chemistry of the atmosphere can be highly affected by lightning discharges due to their large, although quantitatively uncertain, production of nitrogen oxides ($NO_x = NO + NO_2$) (Pickering et al., 2016; Schumann & Huntrieser, 2007; Verma et al., 2021). Being a natural source of NO_x, the extreme temperature from a lightning flash can split N_2 and O_2 and convert them into NO. Then, NO through reaction with peroxyradicals is converted rapidly into NO_2 where, after photolysis to NO and O, the reaction with O_2 leads to a net production of O_3. Lightning NO is also an important source of OH by the reaction with HO_2 (Brune et al., 2021; Labrador et al., 2004), which acts as a catalyst in the oxidation of hydrocarbons and CO leading to the formation of peroxyradicals and HO_2. From 3-D cloud-scale model simulations, Ott et al. (2010) suggest that following convection, a large percentage of LNO_x remains at the altitude where it originated, in the middle and upper troposphere, favorable to O_3 production. Kang et al. (2020) used a model to examine the impact of summertime lightning activity across the U.S. Mountain West States on surface-level O_3. They showed an increase by up to 17 ppb_v in the daily maximum 8-hr O_3, and up to 21 ppb_v in hourly values. Nevertheless, when considering the ozone production by LNO_x in the lifetime of a storm, DeCaria et al. (2005) found very small O_3 production (~2 ppb_v) and Ott et al. (2007) even found a small loss of O_3. Since there is insufficient sunlight inside a storm for the photochemical reactions needed for O_3 production, LNO_x does not seem to be the major source of O_3 during the lifetime of a storm.

Unlike the hot lightning flash channel and its photochemically driven production of ozone via LNOx, ozone can be directly produced in cooler channels and independent of photochemistry, as quantified by Peyrous and Lapeyre (1982). Corona discharges are a type of cold discharge that occurs when energetic electrons and atoms collide (Cooray et al., 2008). From a case study of the inflow and outflow regions of a convective cloud during an aircraft campaign, Bozem et al. (2014) found an imbalance in the ozone budget in the outflow region. They suggested that corona discharges are the most probable source of the O_3 since the entrainment of ozone-rich air and the photochemical production were not enough to close the budget. Similarly, Kotsakis et al. (2017) measured an anomalously large amount of ozone near an electrically convective cloud, and subsequent model simulations confirmed that this ozone was likely produced by corona discharges. Minschwaner et al. (2008) also supported this conclusion, estimating that corona discharges contribute approximately 21% of the ozone production from LNO_x on a global scale, with a significant impact on local ozone budgets. Thus, corona discharges are a potential direct and prompt source of O_3 during storm events.

The fair-weather electric field (E) of the atmosphere is ruled by the Global Electrical Circuit (GEC), which is characterized by a downward current, with the surface being negatively charged and, to be neutral overall, the atmosphere is positive (Haldoupis et al., 2017; Harrison et al., 2020). When layer clouds are present, they act as passive accumulators of charges, while deep convective clouds are considered generators of current. Therefore, to a certain degree, all clouds are electrified (Twomey, 1956). Some studies have explored the relationship between the atmospheric E and its influence on troposphere variables (Israelsson & Oluwafemi, 1975; Latha, 2007; Rycroft et al., 2012). In this study, we assessed how surface ozone concentration varies with the E of storms because the electric field is both a promising source of information and closely related to lightning.

Ozone concentration varies within the atmosphere, both horizontally and vertically. An aircraft campaign (The Regional Carbon Balance in Amazonia–BARCA) conducted over the Amazon Basin revealed that to the west and

north of Manaus, O_3 background values are lower than 20 ppb_v, considered extremely low, during dry-to-wet (November and December 2008) and wet-to-dry (May 2009) seasons (Bela et al., 2015). On the other hand, because of the effect of emissions from biomass burning, leading to O_3 precursors, elevated ozone levels to the east and south of Manaus were seen during the dry-to-wet transition, reaching 40–60 ppb_v. The ozone vertical profile, in turn, increases with height (Logan, 1999) and is strongly affected by downward transport to the surface. Convective downdrafts and ozone enhancements have been reported by several authors, including over the Amazon (e.g., Garstang et al., 1988; Garstang et al., 1990; Scala et al., 1990). Betts et al. (2002) studied four nocturnal events in the Amazon and saw peaks of surface ozone of up to 30 ppb_v, while background values were 3–5 ppb_v, simultaneous with lower values of the equivalent potential temperature (θ_e). The same O_3-θ_e behavior was perceived over the Bay of Bengal. Sahu and Lal (2006) showed an increase (decrease) in ozone (θ_e) of around 13 ppb_v associated with the presence of a convective system, while an increase of around 26 ppb_v was associated with a relatively large-scale convective downdraft event. Not only related to ozone deposition, the downward transport of ozone is also associated with enhancing the oxidation processes of rainforest-emitted volatile organic compounds, the VOCs (Gerken et al., 2016), that can lead to the generation of secondary organic compounds (Ehn et al., 2014), affecting aerosol formation (Wennberg et al., 2018). These studies show that surface ozone concentration is strongly connected to the downward transport of air and it can have an important role in the oxidation reactions near the surface.

The main goal of this study is to demonstrate how surface ozone concentrations respond to variations in the electric field of storms. To this end, we define a research strategy that interrelates it with the evaluation of how downdrafts affect ozone concentration, the incremental ozone production during lightning events, and the development of a parameterization that models ozone concentration during the passage of storms.

2. Data and Methods

The data used are from the central Amazon, collected at the Amazon Tall Tower Observatory (ATTO) site (Andreae et al., 2015). The time series ranges from October 2021 to April 2022. It covers the late dry season and the following wet season, a period of major electrical activity (Albrecht et al., 2011, 2016; Oda et al., 2022; Williams et al., 2002) and near pristine condition (Pöhlker et al., 2016). A combination of ozone concentration, atmospheric electric field, vertical velocity, and cloud top height was used in this study, in addition to satellite lightning data.

Both electric field and vertical velocity/cloud top height instruments are located at the ATTO-Campina site (Machado et al., 2021), located about 4 km from the ATTO site, where ozone data are monitored. Given that thunderstorms in Central Amazonia typically span ~25 km in diameter (Seeley & Romps, 2015), the proximity of these measurement locations ensure they are within the same atmospheric conditions. Regarding time resolution, ozone data are retrieved every 30 min, and for consistency, the maximum values of both the electric field and downdrafts were selected within the same 30-min intervals. This time frame is consistent with the response time for downdrafts in the upper levels to reach the surface.

2.1. Ozone

Ozone data are from an inlet placed above the canopy at a height of 79 m on an 80-m height tower, the INSTANT tower. Concentrations are computed by an Ozone Analyzer (Thermo Environmental Instruments 49i) located in a climatized container at the foot of the tower, that works by pumping air from the sample inlet, measuring O_3 concentration by a direct relationship with the absorption of UV light. The data are given at a time resolution of 30 min, in ppb_v.

2.2. Vertical Velocity and Cloud Top Height

The negative vertical velocity, herein called *downdrafts*, and the cloud top height were obtained from a radar wind profiler, a Scintec LAP3000 (White et al., 2015). The radar operates at 1,290 MHz, with a 7.1° beam width. The velocity obtained is based on the Doppler spectra, which capture oscillations of the refractive index of the air and the relative motion of droplets. The vertical velocity used is characterized by the so-called "Precipitation Mode", which consists of changing the LAP3000 pulses in a similar fashion as in Tridon et al. (2013) to optimize for precipitation measurements. This converts the radar wind profiler to an S-band-like radar and provides the reference mean Doppler velocities, combining air and droplet velocities. These velocities are then a combination

of both the vertical air motion and the terminal velocities of raindrops. Therefore, the downdrafts, as defined in this study, are not merely the vertical air velocities but rather the combined effect of the downward movement of the air and the speed at which drops fall. This approach has been used in the past during the ARM (Atmospheric Radiation Measurement) deployment during GoAmazon 2014/5 (Giangrande et al., 2017; Martin et al., 2016). The height resolution is 420 m, with vertical velocities averaged every 5 min.

In this study, we used data corresponding to the mean velocity in the height range of 1.7–4.5 km, considered the warm layer of the atmosphere in this region, and from 11 to 15 km, considered the glaciated layer. These layers were based on the temperature ranges from Mattos et al. (2017) and the heights were obtained after analyzing multiple radiosondes. The cloud top height was extracted from the highest record of the radar echo.

2.3. Electric Field

The Electric Field Mill (EFM) sensor measures the local atmospheric vertical electric field that corresponds to the negative gradient of the electric potential, E_z. It works by alternately exposing the sensing element, a conductive metallic plate, to the atmospheric electrostatic field and an unloaded reference. The external E charges the sensor board and is subsequently discharged when exposed to the uncharged reference. The charge induced on the sensor board is converted to a voltage through charge amplifiers, this voltage is proportional to the external electric field. The process of exposing (charging) and shielding (discharging) the sensor plate to the electric field is performed by means of a rotating shutter consisting of a mechanically coupled pair of rotors and a motorized stator. As the motor rotates, the shutter alternately opens to allow the external electric field to charge the sensor plate and then closes to protect the sensor plate to discharge it in preparation for the next measurement (Carvalho Magina et al., 2016). The EFM sensor installed at the site is the CS110 model, serial number 1233, manufactured by Campbell Scientific, Inc. coupled to a data logger model CR1000 also manufactured by Campbell Scientific, Inc. Unlike a traditional rotating shutter, the CS110 uses a reciprocating shutter. A stepper motor opens and then closes the reciprocating shutter by 45° during measurements (Campbell Scientific, INC, 2012). The CS110 sensor was calibrated at the factory using the "parallel plate method", where a uniform electric field is developed by applying a known voltage between the parallel plates, resulting in 89.98 m V^{-1} (Volts per meter per millivolt) for the parallel plate multiplier. The site correction factor, which takes into account the height at which the sensor is installed face down, is 0.1031, with the sensor installed at 2 m from the ground, facing downwards, and at a place that minimizes external interference, since the site has multiple instruments and is surrounded by vegetation.

The atmospheric E_z in the presence of clouds can be either negative or positive, depending on the storm charge distribution and its distance from the instrument (MacGorman & Rust, 1998). As the charge within a cloud accumulates, it eventually discharges as lightning, which causes the electric field to drop back to zero. To ease the interpretation, we used the vertical Absolute Electric Field value, herein called $|E_z|$. During clear sky days, the fair-weather $|E_z|$ was between 100 and 200 V m^{-1}. Therefore, our analyses were focused on values higher than 200 V m^{-1}. Ozone concentration during fair-weather occasions was computed and an average of 7.5 ppb_v was found and used as a background value.

2.4. Satellite Lightning

The Geostationary Lightning Mapper (GLM) is an instrument onboard the GOES-16, a Geostationary Operational Satellite. The GLM produces geolocations of lightning flashes in the form of points, with a hierarchy of Flash, Groups, and Events that maps lightning flash extent with spatiotemporal coherency, at an 8 km resolution (Bruning et al., 2019). The satellite's location along the equator and longitude of −75° makes it suitable for continuous monitoring of the lightning activity in the ATTO area due to its proximity to the site (−1.4°, −59°). To obtain a better representation of the lightning activity around ATTO, a very localized place, we used GLM Events, which can approximate the spatial extension of the lightning, instead of GLM Group and Flash, which provide more generalized data about the lightning occurrence. We computed the maximum number of GLM Events in an area of around 50 × 50 km^2, accumulated in 5 min, and used these data for all the analysis. The typical size of thunderstorms is ∼25 km in diameter (Seeley & Romps, 2015), being capable of lasting for a couple of hours (Machado et al., 2018). The EFM has a detection limit of around 20 km in radius (Bloemink, 2013), thus an area of 50 × 50 km^2 has a good representation of thunderstorms around the sensor. To extract the relationship between the number of GLM Events and the values of the $|E_z|$, we computed the maximum value of both variables in a time

interval of 3 hr. Since these storms are usually embedded in cloud clusters with a lifespan of 1.5 hr (Machado et al., 2018), the time interval of 3 hr can capture the whole evolution of such storms.

Classes of $|E_z|$ were determined in a way to encompass similar statistical populations. Starting from 200 V m^{-1}, the classes were set to increase by a fixed factor of 2.5. V m^{-1}. Therefore, the first class spans from 200 to 500 V m^{-1}, the second from 500 to 1,250 V m^{-1}, and the third from 1,250 to 3,125 V m^{-1}.

2.5. Selection of Cases and Linear Regression

In Sections 3.3 and 3.4, case studies are selected based on the $|E_z|$ activity, where one case is defined as consecutive measurements of 5-min-electric field data that have gaps (values below 200 V m^{-1}) not bigger than 15 min. In the analysis, only cases that lasted at least 30 min and were separated by at least 1.5 hr (from beginning and end) from other cases were considered, giving a total of 70 cases.

A multiple linear regression without an intercept was applied to the data of (a) ozone concentration 1.5 hr before the beginning of the case, (b) the highest $|E_z|$ and (c) the strongest downdraft during the case, and (d) the total duration of the case, in order to estimate the ozone concentration during storms. The data were split into two groups with 60% to obtain the regression and 40% to test the model and apply statistical metrics. Different ratios were tested, but showed less accuracy. It is worth mentioning that a LASSO (Tibshirani, 1996) and a Ridge (Hoerl & Kennard, 2000; McDonald, 2009) regression were also tested, but they delivered results that were either similar to or inferior to those from the linear regression model. Therefore, we decided to proceed with the linear regression method.

With the test data (40%), the Mean Square Error (MSE), the MSE with cross-validation with $k = 5$, the Root Mean Squared Error (RMSE), the Mean Squared Logarithmic Error (MSLE), and the R-squared (R^2) were computed. To evaluate the overall significance of the model, the Pearson correlation and the Analysis of Variance (ANOVA) with an F-test (Ståhle & Wold, 1989) and a p-value were computed considering all the data.

The p-value for the F statistic was obtained by using the cumulative distribution function (CDF) of the F-distribution, in addition to the F_{critical} for the case of $p = 0.05$. F_{critical} is the threshold for rejecting the null hypothesis. A high F value indicates that the model explains a significant portion of the variance in the dependent variable, suggesting that the predictors have a meaningful impact. A low F value indicates that the model's explanatory power is similar to a random error. If the F statistic exceeds F_{critical}, we can reject the null hypothesis and conclude that the predictors have a significant effect on the dependent variable.

All the calculations were performed using the Python language, especially making use of the *SciPy.stats* and the *Sklearn* libraries.

3. Results and Discussions

3.1. Ozone, Atmospheric Electric Field, and Downdrafts

Since LNO_x and corona discharges are related to O_3 production, it is a reasonable hypothesis that the degree of storm electrification will be correlated to the ozone concentration. Figure 1a shows this relationship, where a positive correlation between the two variables exists, indicating that surface O_3 variation responds in the same direction to the increase in the $|E_z|$. However, these two variables are interconnected by the occurrence of convective clouds which, in turn, is also connected to vertical motion. Thus, an investigation of cause and effect is discussed in the course of the section.

Downdrafts are responsible for the downward advection of atmospheric properties. Tropospheric O_3 in pristine areas and during the rainy season is produced mainly in the upper troposphere and is transported to the boundary layer by downdrafts (Gerken et al., 2016; Kirchhoff et al., 1990). Ozone concentration increases with height and downdrafts bring rich-ozone air from the free troposphere to the boundary layer. Therefore, with stronger downdrafts, O_3 concentration in the boundary layer is expected to increase.

This transport can be identified in Figure 1b. It is perceived that not only do downdrafts transport O_3 but their magnitudes are also directly related to it. The same behavior found in Figure 1a is also encountered in Figure 1b, with a positive correlation between O_3 and downdraft magnitudes. Weak downdrafts, from −2 to −4 m.s^{-1}, have a mean O_3 concentration of ∼5 ppb_v, while strong downdrafts, from −8 to −10 m.s^{-1}, are characterized by values

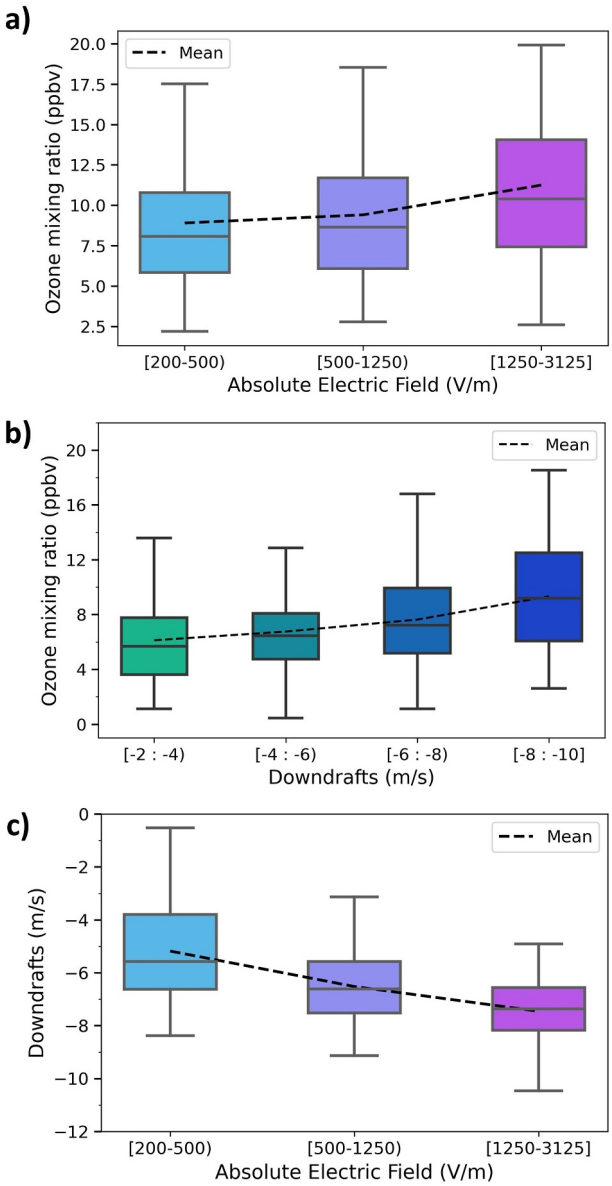

Figure 1. The coupling of the atmospheric electric field, downdrafts (air speed and drop vertical velocity), and ozone. (a) Ozone mixing ratio (ppb_v) distribution for different classes of absolute electric field (V m^{-1}). (b) Ozone mixing ratio distribution for different classes of downdraft magnitudes (m s^{-1}). (c) The distribution of downdrafts for different classes of the absolute value of the electric field.

of ~9 ppb_v. Thus, the strongest downdrafts are in fact related to higher values of surface O_3 concentration. The correlation with the mean values is −0.97 with a p-value of 0.02, showing a statistically significant relationship between the variables. The mean standard deviation of the considered downdraft classes is 3 ppb_v, a large variation given the low mean values. Since we are dealing with a long time series, we must consider that diurnal variation as well as long-range biomass transport of NO_x may affect the variability of O_3 concentration (Bela et al., 2015; Betts et al., 2002). However, long-range transport likely influenced only the months from October to December, as this period marks the transition from the dry (polluted) to wet (clean) season, while the diurnal cycle likely had only a small effect, as most storms occur in the late afternoon. The magnitude of downdrafts is directly linked to the strength of convective clouds (Knupp & Cotton, 1985). Since electrical discharges can produce O_3, the increase in O_3 seen in Figure 1a can be coupled to the strengths of downdrafts. In Figure 1c, the relationship between downdrafts and the $|E_z|$ is shown. It is seen that, in fact, strongest downdrafts are related to the storms being more highly charged. Therefore, the strength of convective clouds is ruling the pattern seen in all three figures. The scatter plots of Figure 1 can be found in Figure S2 of Supporting Information S1.

3.2. The Effect of Lightning Activity on Surface Ozone

Since from Figure 1b, it is seen that the stronger the downdraft, the higher the O_3 concentration, and from Figure 1c, the magnitudes of the downdrafts increase with the $|E_z|$, an interrelationship among these three variables exists. To solve it, an analysis considering O_3 concentration for different classes of downdrafts as a function of the $|E_z|$ was performed (Figure 2a). The result shows that the positive correlation between O_3 and the $|E_z|$ seen in Figure 1a is present for all downdraft classes, with a slight increase as downdraft magnitude increases, except for the weaker downdraft class. Since downdrafts are well correlated to the $|E_z|$ of clouds, the more electrified the clouds, the higher the vertical motions. Clouds more electrified are clouds with deeper vertical development. Downdrafts from around −2 to −4 m s^{-1} appear to not significantly affect surface O_3 concentration. In our study, the downdraft values represent a combination of vertical airspeed and the terminal velocity of raindrops. When we account for the typical raindrop size in Central Amazonas (1–2 mm, Machado et al., 2021) using the Atlas et al. (1973) terminal velocity parameterization, the effective airspeed in these downdrafts is actually closer to −1 m s^{-1}. Thus, although we refer to downdrafts of −4 m s^{-1} in our analysis, this corresponds to an airspeed of approximately −1 m s^{-1} when adjusted by the raindrop terminal velocity.

The computed mean O_3 background for cases of a fair-weather atmosphere was 7.5 ppb_v, whereas, with the $|E_z|$-downdraft-O_3 modulation, there is a computed mean increase ranging from 0.15 to 5.27 ppb_v. Nevertheless, this increase is only significant when the $|E_z|$ is higher, above 1,250 V m^{-1}. It is clear that, for the same downdraft, only when the $|E_z|$ is higher than 1,250 V m^{-1}, is the surface O_3 concentration significantly and exclusively modified by the electric field. Hence, the disentangling of the three variables reveals an O_3 increment at the surface. This increment is not related to the downdraft magnitudes, even though downdrafts strongly influence the overall relationship. The scatter plots of Figure 2 can be found in Figure S3 of Supporting Information S1.

In general, the wet season in central Amazon presents approximately one-third of the rain events as thunderstorms (Machado et al., 2004). On the other hand, all clouds have a degree of electrification, in different orders of magnitude (Twomey, 1956). The electric field gives the electrification degree of the atmosphere, which, at some point, can be related to lightning activity in the area of study. This was found by the analysis of Figures 2b and S1 in Supporting Information S1 showing that, at the ATTO-Campina site, the $|E_z|$ higher than ~1,250 V m^{-1} is

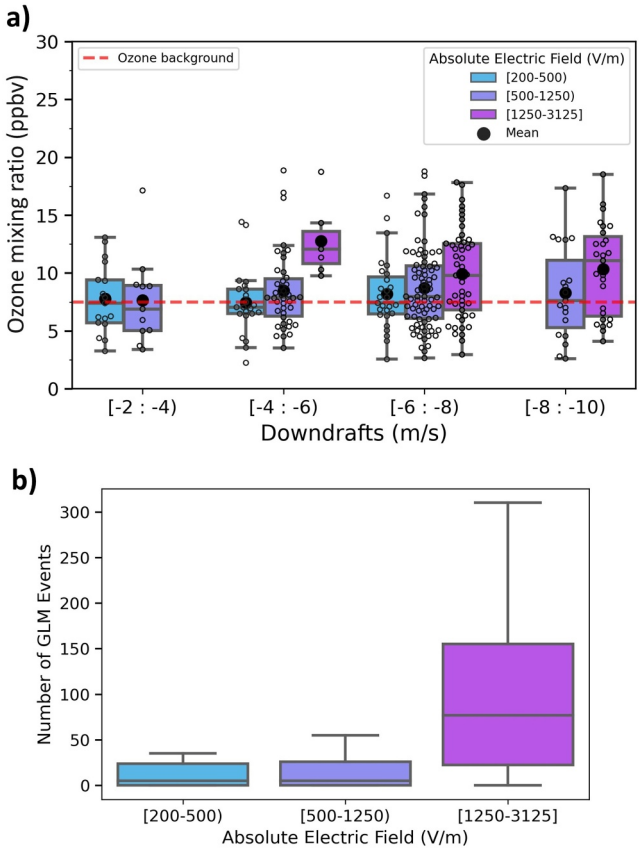

Figure 2. The exploration of cause and effect of the $|E_z|$-downdraft-O_3 coupling. (a) Distribution of ozone mixing ratio (ppb_v) as a function of the absolute electric field (V m^{-1}) for different classes of downdrafts (m s^{-1}) and (b) The number of GLM *Events* for the different classes of absolute electric field (V m^{-1}).

directly associated with lightning activity in the area. The median is greater than 70 lightning GLM Events against a median below 15 for the other $|E_z|$ classes. This value will be used as a lightning threshold in the following analysis.

In Figure S1 of Supporting Information S1, some outliers are observed, which could be explained by the distance of the site from the storm's core. For Figure 2a, from a total of 300 occurrences analyzed, the amount accounted in the >∼1,250 V m^{-1} class represents only 28%. For the other two classes accounting for the majority of the cases ($|E_z|$ < 1,250 V m^{-1}), the possible interpretations for some increase in ozone concentration are: (a) lightning might have happened in a distant area, or (b) the lower $|E_z|$ values were preceded by lightning discharges, showing a cloud loading, or (c) it could be a record of a possible O_3 formation in lower energized environments, from the so-called cold strikes (Cooray et al., 2008), such as corona discharges (Kotsakis et al., 2017).

3.3. Case Studies and Composite Analysis

To explore in detail the coupled system, case studies were performed. The cases were selected according to the electric field activity, where an event is characterized by consecutive occurrences of the $|E_z|$ magnitude (≥200 V m^{-1}) at 5 min. If a magnitude is separated by 15 min or more, it is set as a new case. In the following analysis, only cases that lasted at least 30 min and that were isolated from other cases by 1.5 hr, from the beginning and the end, were taken into account. A total of 70 cases were analyzed.

A crucial understanding was promptly perceived: the position of the site does not always catch the aforementioned effect since the analysis is done in an Eulerian way. The passage of thunderstorms can be either done directly over the site or in the surroundings, which may affect the behavior of the three variables. Other issues worth mentioning are the aging of the thunderstorms when approaching the site, which may impact the amount of ozone produced aloft, the horizontal advection of nearby storms, and the position of the wind profiler radar, which can measure off-axis downdraft regarding ozone production. All of these aspects can contribute to the variability of the results that is apparent in Figures 1 and 2. Some examples of such cases are presented in Figure S4 of Supporting Information S1.

Three cases were selected to represent the three scenarios of the $|E_z|$ classes. Figures 3a, 3b and 3c are of cases that had cloud top heights higher than 12 km, similar ozone background of around 5 ppb_v, similar downdraft magnitudes in the warm layer, around −8 m s^{-1}, and downdrafts also measured up there in the glaciated layer. The difference between them is the maximum $|E_z|$ recorded. Case 1 reached 2,234.01 V m^{-1}, Case 2 reached 925.93 V m^{-1}, and Case 3 reached 417.89 V m^{-1}. The effect of the $|E_z|$ can be clearly seen in the figures. When the thunderstorm approached the site, ozone had an abrupt increase in Case 1, which is the case where $|E_z|$ exceeds the threshold for having lightning discharges, while for Case 2, a slight and continuous increase was seen after the electrical activity, following the unceasing downdrafts. For Case 3, the increase is even lower. The increases in ozone concentration were 6.8, 3.75, and 0.29 ppb_v, respectively. More cases are shown in Figure S5 of Supporting Information S1.

Performing a composite analysis with all 70 cases, the aforementioned effect is present. For every case, ozone concentration was recorded 1.5 hr before and after the beginning and end of the cases. In addition, the maximum ozone concentration, the maximum $|E_z|$, the highest cloud top, and the minimum vertical velocity in the warm layer were selected.

In Figure 4a, ozone concentration is higher for cases under the influence of storms with lightning activity, while for the other two, the increase is lower as the $|E_z|$ decreases. To address the possibility that cloud height influences why clouds with $|E_z|$ > 1,250 V m^{-1} result in higher ground-level ozone due to downward transport from upper

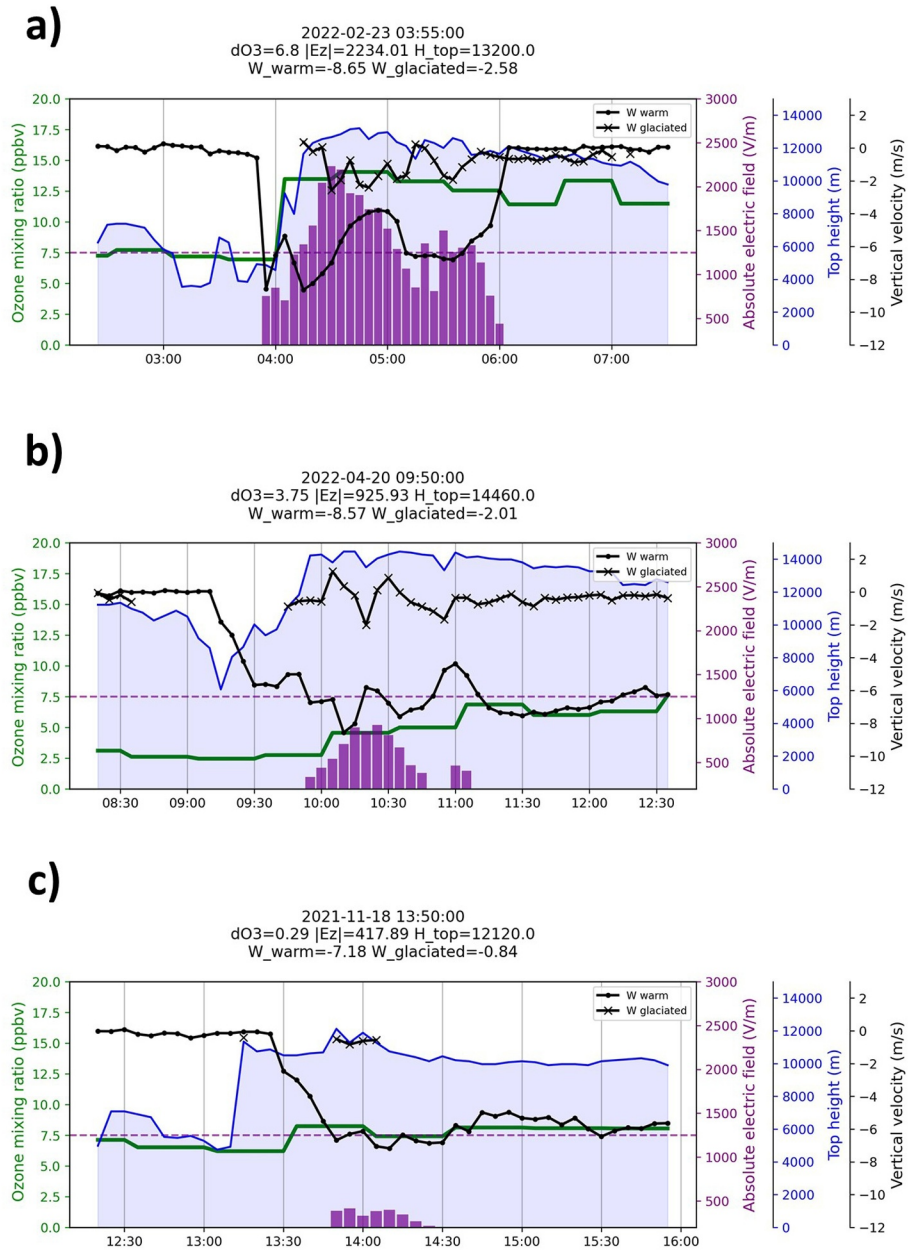

Figure 3. Case studies of storms with atmospheric electric field. All cases had nearly the same conditions of background ozone, downdrafts, and cloud top height, varying only in the degree of the absolute electric field ($|E_z|$). (a) Case 1: strong $|E_z|$, (b) Case 2: moderate $|E_z|$, and (c) Case 3: weak $|E_z|$. Only negative vertical velocities were plotted. The black lines refer to the mean vertical velocity in the warm layer (W_{warm}; 1.7–4.5 km) and the glaciated layer ($W_{glaciated}$; 10–15 km), the blue line is the cloud top height in meters, the purple bars are the $|E_z|$ values, including the dashed line delimiting the threshold for lightning activity, and the green line is the ozone mixing ratio. The title summarizes each case, showing the ozone increment (dO3), the highest $|E_z|$ and cloud top height, and the strongest downdrafts in the warm and the glaciated layer.

levels, analyses including cloud height were conducted. Figures 4b and 4c show that clouds with a top higher than 10 km present indeed the strongest downdrafts and the highest ozone increase when $|E_z| > 1{,}250$ V m^{-1}. However, there are also significant increases in ozone when $|E_z| < 1{,}250$ V m^{-1}, even though downdrafts are weaker or cloud tops are lower. This means that something else must be influencing the ozone concentration. It may be dominated by the effect of corona discharges. To conclude the statement, the analysis considering only clouds with the highest tops (12–15 km) and strongest downdrafts (-10 to -7 m s^{-1}) assures the increment of ozone due

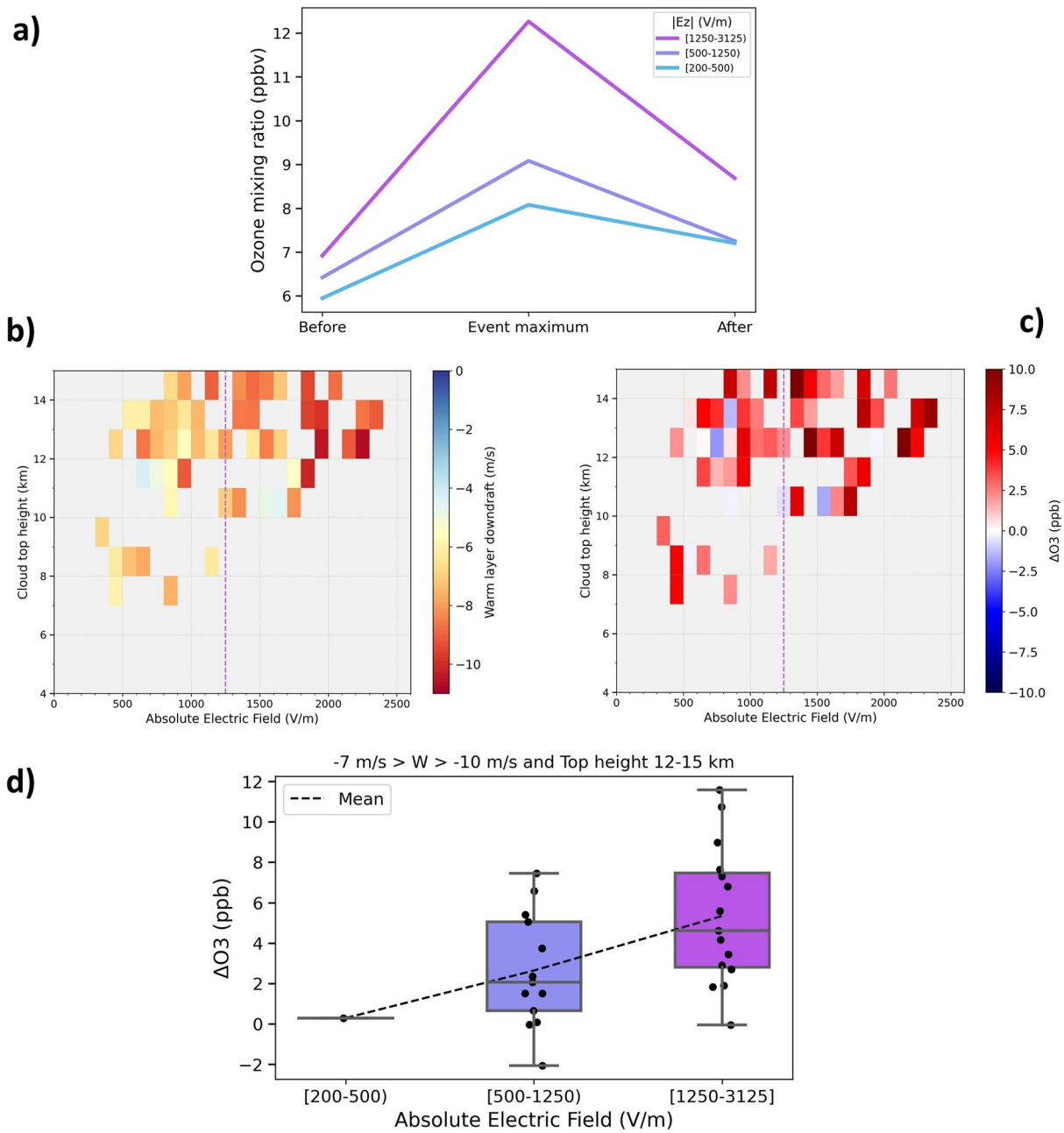

Figure 4. Composite analysis of the cases. (a) Mean ozone variation 1.5 hr before, at the maximum activity of the absolute electric field ($|E_z|$), and 1.5 hr after the end of the events, (b) the distribution of the downdraft in the warm layer regarding cloud top height and $|E_z|$, (c) the distribution of the variation in ozone (delta O3) regarding cloud top height and $|E_z|$, and (d) boxplot of the variation in ozone for the three classes of $|E_z|$ in extreme cases where downdrafts in the warm layer were between −10 and −7 m s^{-1} and cloud top height between 12 and 15 km.

to electrical activity, such an increment that is not an effect of how strong a downdraft is or how high a cloud is (Figure 4d).

3.4. A Parameterization for Estimating Ozone During Storms

From the selected 70 cases, a model to estimate the ozone concentration during the occurrence of a storm was obtained. The data set was split into training and testing sets using a 60–40 split ratio to ensure robust model evaluation. The model takes the initial ozone concentration 1.5 hr before the event ($O_{3,i}$), the highest $|E_z|$ and the strongest downdraft of the mean values in the warm layer of the atmosphere (W_{warm}) during the event, and the

Table 1
Evaluation of the Model

Test data (40%)			*MSE*			7.99 ppb_v^2			
			MSE (k = 5)			9.65 ppb_v^2			
			RMSE			2.83 ppb_v			
			MSLE			0.0623			
			R^2			0.41			
All data			*Pearson*			0.66			
			F-test			11.82			
			P-value			0.0000			
Cases	$O_{3,i}$ (ppb_v)	$\|E_z\|$ (V m^{-1})	W_{warm} (m s^{-1})	dt (min)	$dO_{3,obs}$ (ppb_v)	$dO_{3,model}$ (ppb_v)	$\|E_z\|$ (%)	W_{warm} (%)	Ratio $\|E_z\|/W_{warm}$
1	7.25	2234	−8.65	125	6.80	5.88	32.3	16.0	2:1
2	3.10	925	−8.57	75	3.75	3.91	25.1	29.6	1:1
3	7.12	417	−7.18	35	0.29	0.97	9.8	21.5	1:2

Note. The first two parts show the statistic metrics when using the testing and all data. MSE stands for Mean Square Error and *k* is the number of cross-validations, RMSE stands for the Root Mean Squared Error, MSLE stands for Mean Squared Logarithmic Error, R^2 is R-squared. The Pearson coefficient and the *F*-test and P-value were used for evaluating the model with the full data set. The third part shows the variables for each case, with initial ozone ($O_{3,i}$), absolute electric field ($|E_z|$), downdraft in the warm layer (W_{warm}), and the duration of the event (dt). The observed and modeled increases in ozone are shown as $dO_{3,obs,}$ and $dO_{3,model}$. Following, the percentage of contribution of $|E_z|$ and W_{warm} to the increase in ozone and the respective ratio.

event duration (*dt*) as the variables to estimate the ozone concentration at the surface (Equation 1). The duration of the event is used as a weight to account for the number of lightning discharges, as longer durations mean more electrical activity. An equation for converting GLM Events (the maximum number of events within 3 hr in the area of 50 × 50 km^2) into $|E_z|$ is shown in Equation 2. The equation was extracted by the relationship plotted in Figure S1 of Supporting Information S1, providing an alternative approach for utilizing the parameterization.

$$O_{3,\text{storm}} = 0.7180 \times O_{3,i} + 0.0019 \times \left|E_z\right| - 0.2423 \times W_{\text{warm}} + 0.0127 \times dt \quad (1)$$

$$\left|E_z\right| = 550 \times \log(\text{GLM\_Events} \times 0.115) \quad (2)$$

The testing data were used to obtain the first chain of statistical metrics presented in Table 1. The Mean Square Error (MSE) presents a value of 7.99 ppb_v^2 which indicates the average squared difference between the observed and predicted ozone concentrations. When using 5-fold cross-validation, the MSE slightly increases to 9.65 ppb_v^2, suggesting a minor variance in the model performance across different subsets of the data. The Root Mean Squared Error (RMSE) indicates that, on average, the model's predictions deviate by approximately 2.83 ppb_v from the observed values. The Mean Squared Logarithmic Error (MSLE) of 0.0623 is relatively low, indicating that the model performs effectively when the target variable's distribution is log-transformed, showing that it can make predictions that are proportional to the actual values, rather than being heavily influenced by extreme values. The R-squared (R^2) value of 0.41 indicates that there is a moderate level of explanatory power by the model.

When implementing all observed variables into the model, the Pearson coefficient of 0.66 shows that the model's result has a moderate positive linear relationship against the observed data. In addition, the analysis of variance (ANOVA) reveals that the model is highly significant. The *F*-test of 11.82 substantially exceeds the $F_{critical}$ of 2.51 at the 0.05 significance level, demonstrating that the variability explained by the regression model is significantly greater than the unexplained variability, leading us to reject the null hypothesis that all regression coefficients are equal to zero. Furthermore, the associated p-value is 0.0000, which is extremely low, underscoring the improbability that these results occurred by chance. Together, these metrics affirm that the model is highly significant, meaning that the independent variables included in the regression have a substantial and statistically significant impact on the dependent variable. This suggests that the predictors used in the model effectively explain the ozone variation, providing strong evidence for the robustness of the model's predictive power. The scatter plot in Figure 5 reinforces it as most of the modeled ozone follows the best line, although there seems to be

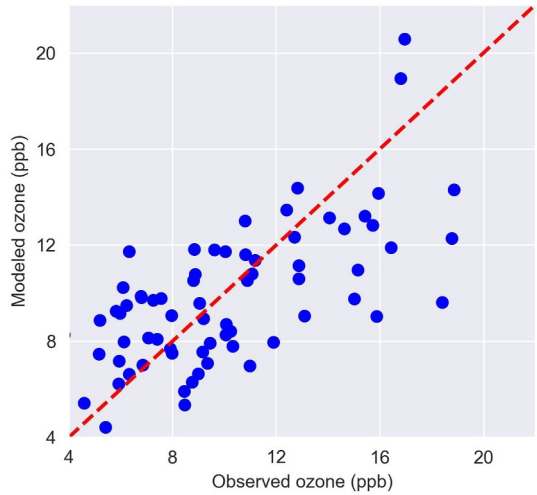

Figure 5. The scatter plot of the observed and modeled ozone concentration during storms. The red dashed line is the identity line.

an overestimation in concentrations below 8 ppb_v and an underestimation for values higher than 14 ppb_v. However, there are cases where the model predicted well in these ranges. As previously mentioned, the Eulerian approach may not fully capture the dynamic and heterogeneous nature of atmospheric processes that affect the ozone concentration during the passage of storms, possibly contributing to the scattered data. The applicability of this equation to non-tropical regions and during the dry season would need to be validated. However, the equation has an initial ozone concentration, taking into account the ozone background. At the same time, as mentioned in the text, ozone production is mainly due to the corona discharge, so we do not expect large seasonal differences due to NO_x variability.

As a first approach to estimating the ozone concentration and the proportional contribution of each variable, the presented model is satisfactory. The model intends to not only model the ozone concentration but also to further account for the increment due to electrical activity. When applying the three cases of Figure 3 to the model, it captures reasonably well the increase in ozone concentration ($dO_{3,obs}$ vs. $dO_{3,model}$).

From Table 1, in Case 1, the $|E_z|$ has double the influence on the increase in ozone when compared with downdrafts, a ratio of 2:1. For Case 2, both the electrical activity and the downdrafts contribute equally to the increase in ozone concentration (1:1 ratio). While for Case 3, the effects of downdrafts dominate (1:2 ratio). To understand how the variation of this ratio is and the influence of each of the two variables on the increase of ozone, we applied to the equation downdrafts varying from -10 to -4 m s^{-1} and $|E_z|$ from 200 to 3,125 V m^{-1}, while assuming an initial background ozone of 7.5 ppb_v and a typical storm duration of 60 min.

Figure 6 illustrates the total increase in ozone (blue lines) and the contribution ratio of $|E_z|$ to downdrafts (red lines). The equation aligns well with the observed effects of lightning. It is first seen that it fitted surprisingly well the effects of lightning discussed in the previous sections, as the contribution of the $|E_z|$ starts to dominate from around 1,250 V m^{-1} on (1:1), regardless of strong downdrafts, and it doubles when $|E_z|$ exceeds 2,500 V m^{-1} even

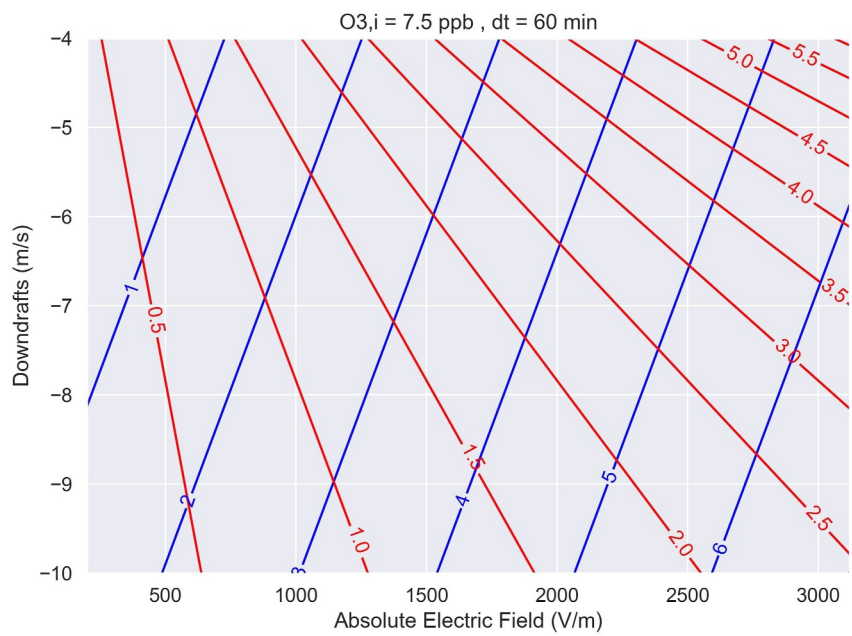

Figure 6. Accounting for the effects of the absolute electric field and downdrafts in the ozone increase. Initial ozone and event duration were fixed at 7.5 ppb_v and 60 min, respectively. Blue lines indicate the change in ozone (delta O3), while red lines represent the ratio of the contribution of the absolute electric field ($|E_z|$) to that of downdrafts.

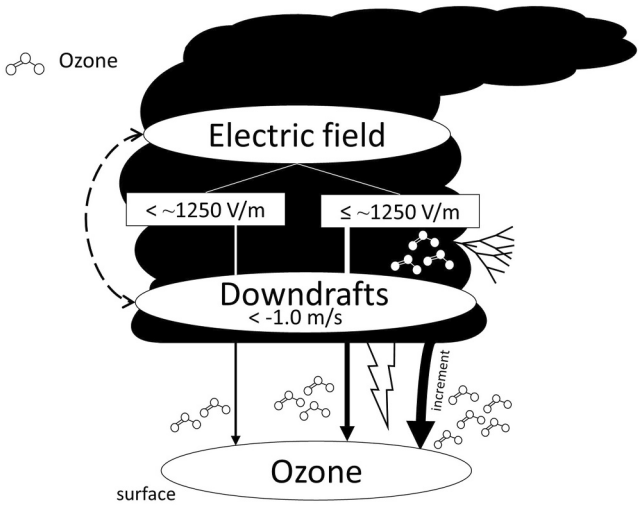

Figure 7. Diagram of the coupled $|E_z|$-downdrafts-O_3 system. The dashed arrow represents the positive feedback between the variables, which is caused by their association with the invigoration of convective clouds. Solid arrows represent the downward transport of ozone. The thicker the line, the more is ozone at the surface, with an increment due to lightning activity. The electric field is in absolute value.

with strong downdrafts (2:1). This shows that the equation is satisfactory in accounting for the effects of cloud electrification on the increase of ozone. Lower $|E_z|$ values shift the dominance to downdrafts, achieving a ratio of 1:2 or more. The individual areas of influence of both variables can be checked in Figures S6a and S6b of Supporting Information S1, highlighted in Figure S6c of Supporting Information S1. The total increase of ozone can reach a minimum of 3 ppb_v in the case of strong downdrafts and initial lightning activity, rising to over 6 ppb_v as $|E_z|$ increases. In the downdraft-dominated range, the increase can be up to 3 ppb_v.

4. Summary and Conclusions

In this study, we investigated the effects of cloud electrification on surface ozone concentration in the central Amazon. The two variables were found to be positively correlated, and the main cause is attributable to downdrafts. The cloud electric field and the downdrafts are interconnected to convective clouds, having a positive correlation as a function of the invigoration of these clouds. Due to downdrafts, ozone near the surface increases with the increasing magnitudes of the downward advection, which leads to ozone also showing a positive response with the increase in the cloud electric field. This finding revealed that surface ozone concentration, cloud electrification, and downdrafts are a coupled system. The disentangling of this coupling has revealed that downdrafts modulate surface ozone concentration; however, there is also an increment of ozone that is not related to the downdrafts' magnitudes or cloud top heights, but instead, to the highly electrified regions aloft to the surface. For an absolute electric field higher than ~1,250 V m^{-1}, no matter the downdrafts magnitudes, we found a mean maximum ozone increment of about 5.0 ppb_v. This threshold of the absolute electric field was found to be directly linked to lightning activity, which can exhibit a 2:1 ratio or more in the increase of surface ozone compared to downdrafts. Therefore, the more electrified the clouds are, the greater the ozone increment at the surface. Our study cannot indicate the specific contribution of each ozone-production mechanism, but based on the literature, corona discharge is possibly the main source since we dealt with O_3 production during the lifetime of storms. Below 1,250 V m^{-1}, not directly associated with lightning activity, the proportion can change to 1:2 or more, where ozone increment can be less prominent, being strongly connected to the modulation of downdrafts stronger than −4m s^{-1}. Since this downdraft is the combination of airspeed and terminal velocity of droplets, its actual value considering the typical raindrop size in Amazon, is around −1 m s^{-1}. Further investigation must be done since cold strikes, like corona discharges, could be a source of ozone in less energized environments.

In Figure 7 we present a schematic summary of the processes investigated. The dashed arrow illustrates a positive correlation between the absolute electric field ($|E_z|$) and downdrafts, mediated by the strength of convective clouds: as one increases, the other follows suit. Downdrafts stronger than −1 m s^{-1} modulate ozone at the surface as they increase in magnitude. The solid arrows show the downward advection of ozone, increasing in magnitude with the arrow thickness. An increment in ozone at the surface is indicated. It happens when the $|E_z|$ is around or higher than 1,250 V m^{-1}, directly related to lightning activity. Corona discharges are also represented, along with its ozone-related production.

We derived a parameterization for ozone concentration during the occurrence of storms by using the ozone concentration before the event, the maximum absolute electric field and the downdraft in the warm layer of the atmosphere during the event, and the total duration of the event. The statistically significant equation effectively accounts for the proportional impacts of both electricity and downdrafts on surface ozone levels, demonstrating a good potential predictive capability and offering a valuable tool for atmospheric models. We also provide an equation for converting GLM Events into the absolute electric field for a more direct application in the models.

Data Availability Statement

All data used in the study are available with open access at Edmond repository and can be accessed at https://doi.org/10.17617/3.5S5XUV (Unfer et al., 2023).

Acknowledgments

This research was funded by the São Paulo Research Foundation (FAPESP), Grants 2021/03547-7, 2022/01780-9, 2022/07974-0, by the EU MSCA Doctoral Network CLOUD-DOC 101073026, by the Coordenação de Aperfeiçoamento de Pessoal de Nível Superior—Brasil (CAPES)—Finance Code 001, by the Bundesministerium für Bildung und Forschung (BMBF contracts 01LB1001A, 01LK1602B, and 01LK2101B), by the Brazilian Ministério da Ciência, Tecnologia e Inovação (MCTI/FINEP contract 01.11.01248.00), by the Conselho Nacional de Desenvolvimento Científico e Tecnológico (CNPq), Grants 440171/2022-9 and 438638/2018-2, by the Serrapilheira, Grant 2211-41823, and by the Max Planck Society. For the operation of the ATTO site, we acknowledge the support of the Instituto Nacional de Pesquisas da Amazônia (INPA), the Amazon State University (UEA), the Large-Scale Biosphere-Atmosphere Experiment (LBA), FAPEAM, the Reserva de Desenvolvimento Sustentável do Uatumã (SDS/CEUC/RDS-Uatumã), and the Max Planck Society. Particularly, we would like to thank the ATTO-Campina team involved in the technical, logistical, and scientific support. We would like to acknowledge the three anonymous reviewers for their valuable comments and suggestions, which greatly contributed to improving the quality of our manuscript. Open Access funding enabled and organized by Projekt DEAL.

References

Albrecht, R. I., Goodman, S. J., Buechler, D. E., Blakeslee, R. J., & Christian, H. J. (2016). Where are the lightning hotspots on earth? *Bulletin of the American Meteorological Society*, *97*(11), 2051–2068. https://doi.org/10.1175/BAMS-D-14-00193.1

Albrecht, R. I., Morales, C. A., & Silva Dias, M. A. F. (2011). Electrification of precipitating systems over the Amazon: Physical processes of thunderstorm development. *Journal of Geophysical Research*, *116*(D8), D08209. https://doi.org/10.1029/2010JD014756

Andreae, M. O., Acevedo, O. C., Araújo, A., Artaxo, P., Barbosa, C. G. G., Barbosa, H. M. J., et al. (2015). The Amazon Tall Tower Observatory (ATTO): Overview of pilot measurements on ecosystem ecology, meteorology, trace gases, and aerosols. *Atmospheric Chemistry and Physics*, *15*(18), 10723–10776. https://doi.org/10.5194/acp-15-10723-2015

Atlas, D., Srivastava, R. C., & Sekhon, R. S. (1973). Doppler radar characteristics of precipitation at vertical incidence. *Review of Geophysics*, *11*(1), 1–35. https://doi.org/10.1029/RG011i001p00001

Bela, M. M., Longo, K. M., Freitas, S. R., Moreira, D. S., Beck, V., Wofsy, S. C., et al. (2015). Ozone production and transport over the Amazon Basin during the dry-to-wet and wet-to-dry transition seasons. *Atmospheric Chemistry and Physics*, *15*(2), 757–782. https://doi.org/10.5194/acp-15-757-2015

Betts, A. K., Gatti, L. V., Cordova, A. M., Silva Dias, M. A. F., & Fuentes, J. D. (2002). Transport of ozone to the surface by convective downdrafts at night. *Journal of Geophysical Research*, *107*(D20), 8046. https://doi.org/10.1029/2000JD000158

Bloemink, H. (2013). *Static electricity measurements for lightning warnings – an exploration (Internal Report IR-2013-01)*. De Bilt: Royal Netherlands Meteorological Institute.

Bozem, H., Fischer, H., Gurk, C., Schiller, C. L., Parchatka, U., Koenigstedt, R., et al. (2014). Influence of corona discharge on the ozone budget in the tropical free troposphere: A case study of deep convection during GABRIEL. *Atmospheric Chemistry and Physics*, *14*(17), 8917–8931. https://doi.org/10.5194/acp-14-8917-2014

Bray, C. D., Battye, W. H., Aneja, V. P., & Schlesinger, W. H. (2021). Global emissions of NH_3, NOx, and N_2O from biomass burning and the impact of climate change. *Journal of the Air & Waste Management Association*, *71*(1), 102–114. https://doi.org/10.1080/10962247.2020.1842822

Brune, W. H., McFarland, P. J., Bruning, E., Waugh, S., MacGorman, D., Miller, D. O., et al. (2021). Extreme oxidant amounts produced by lightning in storm clouds. *Science*, *372*(6543), 711–715. https://doi.org/10.1126/science.abg0492

Bruning, E. C., Tillier, C. E., Edgington, S. F., Rudlosky, S. D., Zajic, J., Gravelle, C., et al. (2019). Meteorological imagery for the geostationary lightning mapper. *Journal of Geophysical Research: Atmospheres*, *124*(24), 14285–14309. https://doi.org/10.1029/2019JD030874

Bucsela, E. J., Pickering, K. E., Huntemann, T. L., Cohen, R. C., Perring, A., Gleason, J. F., et al. (2010). Lightning-generated NOx seen by the ozone monitoring instrument during NASA's tropical composition, cloud and climate coupling experiment (TC_4). *Journal of Geophysical Research*, *115*(D10), D00J10. https://doi.org/10.1029/2009jd013118

Campbell Scientific, INC. (2012). CS110 electric field meter (revision 4/12).

Carvalho Magina, F., Junior, O. P., & Naccarato, K. P. (2016). Atmospheric electric field Sensors Network integration in Brazi. *IEEE Latin America Transactions*, *14*, 3056–3064. https://doi.org/10.1109/TLA.2016.7587602

Clark, S. K., Ward, D. S., & Mahowald, N. M. (2017). Parameterization-based uncertainty in future lightning flash density. *Geophysical Research Letters*, *44*(6), 2893–2901. https://doi.org/10.1002/2017GL073017

Cooray, V., Becerra, M., & Rahman, M. (2008). On the NO_x generation in corona, streamer and low pressure electrical discharges. *The Open Atmospheric Science Journal*, *2*(1), 176–180. https://doi.org/10.2174/1874282300802010176

DeCaria, A. J., Pickering, K. E., Stenchikov, G. L., & Ott, L. E. (2005). Lightning-generated NOX and its impact on tropospheric ozone production: A three-dimensional modeling study of a Stratosphere-Troposphere Experiment: Radiation, Aerosols and Ozone (STERAO-A) thunderstorm. *Journal of Geophysical Research*, *110*(D14), D14303. https://doi.org/10.1029/2004JD005556

Ehn, M., Thornton, J. A., Kleist, E., Sipilä, M., Junninen, H., Pullinen, I., et al. (2014). A large source of low-volatility secondary organic aerosol. *Nature*, *506*(7489), 476–479. https://doi.org/10.1038/nature13032

Finney, D. L., Doherty, R. M., Wild, O., & Abraham, N. L. (2016). The impact of lightning on tropospheric ozone chemistry using a new global lightning parametrization. *Atmospheric Chemistry and Physics*, *16*(12), 7507–7522. https://doi.org/10.5194/acp-16-7507-2016

Finney, D. L., Doherty, R. M., Wild, O., Stevenson, D. S., MacKenzie, I. A., & Blyth, A. M. (2018). A projected decrease in lightning under climate change. *Nature Climate Change*, *8*(3), 210–213. https://doi.org/10.1038/s41558-018-0072-6

Garstang, M., Scala, J., Greco, S., Harriss, R., Beck, S., Browell, E., et al. (1988). Trace gas exchanges and convective transports over the Amazonian rain forest. *Journal of Geophysical Research*, *93*(D2), 1528–1550. https://doi.org/10.1029/JD093iD02p01528

Garstang, M., Ulanski, S., Greco, S., Scala, J., Swap, R., Fitzjarrald, D., et al. (1990). The Amazon Boundary-Layer Experiment (ABLE 2B): A meteorological perspective. *Bulletin of the American Meteorological Society*, *71*(1), 19–32. https://doi.org/10.1175/1520-0477(1990)071<0019:TABLEA>2.0.CO;2

Gerken, T., Wei, D., Chase, R. J., Fuentes, J. D., Schumacher, C., Machado, L. A. T., et al. (2016). Downward transport of ozone rich air and implications for atmospheric chemistry in the Amazon rainforest. *Atmospheric Environment*, *124*(Part A), 64–76. https://doi.org/10.1016/j.atmosenv.2015.11.014

Giangrande, S. E., Feng, Z., Jensen, M. P., Comstock, J. M., Johnson, K. L., Toto, T., et al. (2017). Cloud characteristics, thermodynamic controls and radiative impacts during the observations and modeling of the Green Ocean Amazon (GoAmazon2014/5) experiment. *Atmospheric Chemistry and Physics*, *17*(23), 14519–14541. https://doi.org/10.5194/acp-17-14519-2017

Grewe, V., Dahlmann, K., Matthes, S., & Steinbrecht, W. (2012). Attributing ozone to NOx emissions: Implications for climate mitigation measures. *Atmospheric Environment*, *59*, 102–107. https://doi.org/10.1016/j.atmosenv.2012.05.002

Haldoupis, C., Rycroft, M., Williams, E., & Price, C. (2017). Is the "Earth-ionosphere capacitor" a valid component in the atmospheric global electric circuit? *Journal of Atmospheric and Solar-Terrestrial Physics*, *164*, 127–131. https://doi.org/10.1016/j.jastp.2017.08.012

Harrison, R. G., Nicoll, K. A., Mareev, E., Slyunyaev, N., & Rycroft, M. J. (2020). Extensive layer clouds in the global electric circuit: Their effects on vertical charge distribution and storage. *Proceedings of the Royal Society A*, *476*(2238), 20190758. https://doi.org/10.1098/rspa.2019.0758

Hoerl, A. E., & Kennard, R. W. (2000). Ridge regression: Biased estimation for nonorthogonal problems. *Technometrics*, *42*(1), 80–86. https://doi.org/10.2307/1271436

Israelsson, S., & Oluwafemi, C. (1975). Power and cross-power spectral studies of electric and meteorological parameters under fair weather conditions in the atmospheric surface layer. *Boundary-Layer Meteorology*, *9*(4), 461–477. https://doi.org/10.1007/BF00223394

Kang, D., Mathur, R., Pouliot, G. A., Gilliam, R. C., & Wong, D. C. (2020). Significant ground-level ozone attributed to lightning-induced nitrogen oxides during summertime over the Mountain West States. *npj Climate and Atmospheric Science*, *3*(1), 6. https://doi.org/10.1038/s41612-020-0108-2

Karagodin-Doyennel, A., Rozanov, E., Sukhodolov, T., Egorova, T., Sedlacek, J., & Peter, T. (2023). The future ozone trends in changing climate simulated with SOCOLv4. *Atmospheric Chemistry and Physics*, *23*(8), 4801–4817. https://doi.org/10.5194/acp-23-4801-2023

Kirchhoff, V. W. J. H., da Silva, I. M. O., & Browell, E. V. (1990). Ozone measurements in Amazonia: Dry season versus wet season. *Journal of Geophysical Research*, *95*(D10), 16913–16926. https://doi.org/10.1029/JD095iD10p16913

Knupp, K. R., & Cotton, W. R. (1985). Convective cloud downdraft structure: An interpretive survey. *Reviews of Geophysics*, *23*(2), 183–215. https://doi.org/10.1029/RG023i002p00183

Kotsakis, A., Morris, G. A., Lefer, B., Jeon, W., Roy, A., Minschwaner, K., et al. (2017). Ozone production by corona discharges during a convective event in DISCOVER-AQ Houston. *Atmospheric Environment*, *161*, 13–17. https://doi.org/10.1016/j.atmosenv.2017.04.018

Labrador, L. J., von Kuhlmann, R., & Lawrence, M. G. (2004). Strong sensitivity of the global mean OH concentration and the tropospheric oxidizing efficiency to the source of NOx from lightning. *Geophysical Research Letters*, *31*(6), L06102. https://doi.org/10.1029/2003GL019229

Latha, R. (2007). Micrometeorological influences and surface layer radon ion production: Consequences for the atmospheric electric field. *Atmospheric Environment*, *41*(4), 867–877. https://doi.org/10.1016/j.atmosenv.2006.07.051

Lelieveld, J., Dentener, F. J., Peters, W., & Krol, M. C. (2004). On the role of hydroxyl radicals in the self-cleansing capacity of the troposphere. *Atmospheric Chemistry and Physics*, *4*(9/10), 2337–2344. https://doi.org/10.5194/acp-4-2337-2004

Logan, J. A. (1999). An analysis of ozonesonde data for the troposphere: Recommendations for testing 3-D models and development of a gridded climatology for tropospheric ozone. *Journal of Geophysical Research*, *104*(D13), 16115–16149. https://doi.org/10.1029/1998JD100096

Logan, J. A., Prather, M. J., Wofsy, S. C., & Mcelroy, M. B. (1981). Tropospheric chemistry: A global perspective. *Journal of Geophysical Research*, *86*(C8), 7210–7254. https://doi.org/10.1029/JC086iC08p07210

Lu, X., Zhang, L., & Shen, L. (2019). Meteorology and climate influences on tropospheric ozone: A review of natural sources, chemistry, and transport patterns. *Current Pollution Reports*, *5*(4), 238–260. https://doi.org/10.1007/s40726-019-00118-3

MacGorman, D. R., & Rust, W. D. (1998). *The electrical nature of storms*. Oxford University Press.

Machado, L., Laurent, H., Dessay, N., & Miranda, I. (2004). Seasonal and diurnal variability of convection over the Amazonia: A comparison of different vegetation types and large scale forcing. *Theoretical and Applied Climatology*, *78*(1–3), 61–77. https://doi.org/10.1007/s00704-004-0044-9

Machado, L. A. T., Calheiros, A. J. P., Biscaro, T., Giangrande, S., Silva Dias, M. A. F., Cecchini, M. A., et al. (2018). Overview: Precipitation characteristics and sensitivities to environmental conditions during GoAmazon 2014/5 and ACRIDICON-CHUVA. *Atmospheric Chemistry and Physics*, *18*(9), 6461–6482. https://doi.org/10.5194/acp-18-6461-2018

Machado, L. A. T., Franco, M. A., Kremper, L. A., Ditas, F., Andreae, M. O., Artaxo, P., et al. (2021). How weather events modify aerosol particle size distributions in the Amazon boundary layer. *Atmospheric Chemistry and Physics*, *21*(23), 18065–18086. https://doi.org/10.5194/acp-21-18065-2021

Martin, R. V., Jacob, D. J., Logan, J. A., Ziemke, J. M., & Washington, R. (2000). Detection of a lightning influence on tropical tropospheric ozone. *Geophysical Research Letters*, *27*(11), 1639–1842. https://doi.org/10.1029/1999GL011181

Martin, S. T., Artaxo, P., Machado, L. A. T., Manzi, A. O., Souza, R. A. F., Schumacher, C., et al. (2016). Introduction: Observations and modeling of the green ocean Amazon (GoAmazon2014/5). *Atmospheric Chemistry and Physics*, *16*(8), 4785–4797. https://doi.org/10.5194/acp-16-4785-2016

Mattos, E. V., Machado, L. A. T., Williams, E. R., Goodman, S. J., Blakeslee, R. J., & Bailey, J. C. (2017). Electrification life cycle of incipient thunderstorms. *Journal of Geophysical Research Atmosphere*, *122*(8), 4670–4697. https://doi.org/10.1002/2016jd025772

McDonald, G. C. (2009). Ridge regression. *WIREs Computational Statistics*, *1*, 93–100. https://doi.org/10.1002/wics.14

McGrath, W. D., & Norrish, R. G. W. (1958). Influence of water on the photolytic decomposition of ozone. *Nature*, *182*(4630), 235–237. https://doi.org/10.1038/182235a0

Minschwaner, K., Kalnajs, L. E., Dubey, M. K., Avallone, L. M., Sawaengphokai, P. C., Edens, H. E., & Winn, W. P. (2008). Observation of enhanced ozone in an electrically active storm over Socorro, NM: Implications for ozone production from corona discharges. *Journal of Geophysical Research*, *113*(D17), D17208. https://doi.org/10.1029/2007JD009500

Nguyen, D. H., Lin, C., Vu, C. T., Cheruiyot, N. K., Nguyen, M. K., Le, T. H., et al. (2022). Tropospheric ozone and NOx: A review of worldwide variation and meteorological influences. *Environmental Technology and Innovation*, *28*, 102809. https://doi.org/10.1016/j.eti.2022.102809

Oda, P. S. S., Enoré, D. P., Mattos, E. V., Gonçalves, W. A., & Albrecht, R. I. (2022). An initial assessment of the distribution of Total flash Rate Density (FRD) in Brazil from GOES-16 Geostationary lightning Mapper (GLM) observations. *Atmospheric Research*, *270*, 106081. https://doi.org/10.1016/j.atmosres.2022.106081

Ott, L. E., Pickering, K. E., Stenchikov, G. L., Allen, D. J., DeCaria, A. J., Ridley, B., et al. (2010). Production of lightning NOx and its vertical distribution calculated from three-dimensional cloud-scale chemical transport model simulations. *Journal of Geophysical Research*, *115*(D4), D04301. https://doi.org/10.1029/2009JD011880

Ott, L. E., Pickering, K. E., Stenchikov, G. L., Huntrieser, H., & Schumann, U. (2007). Effects of lightning NOx production during the 21 July European Lightning Nitrogen Oxides Project storm studied with a three-dimensional cloud-scale chemical transport model. *Journal of Geophysical Research*, *112*(D5), D05307. https://doi.org/10.1029/2006JD007365

Patra, P. K., Krol, M. C., Montzka, S. A., Arnold, T., Atlas, E. L., Lintner, B. R., et al. (2014). Observational evidence for interhemispheric hydroxyl-radical parity. *Nature*, *513*(7517), 219–223. https://doi.org/10.1038/nature13721

Peyrous, R., & Lapeyre, R.-M. (1982). Gaseous products created by electrical discharges in the atmosphere and condensation nuclei resulting from gaseous phase reactions. *Atmospheric Environment*, *16*(5), 959–3907. https://doi.org/10.1016/0004-6981(82)90182-2

Pickering, K. E., Bucsela, E., Allen, D., Ring, A., Holzworth, R., & Krotkov, N. (2016). Estimates of lightning NOx production based on OMI NO_2 observations over the Gulf of Mexico. *Journal of Geophysical Research: Atmospheres*, *121*(14), 8668–8691. https://doi.org/10.1002/2015JD024179

Pinto Junior, O., & Pinto, I. (2020). Lightning changes in response to global warming in Rio de Janeiro, Brazil. *American Journal of Climate Change*, *9*, 266–273. https://doi.org/10.4236/ajcc.2020.93017

Pöhlker, M. L., Pöhlker, C., Ditas, F., Klimach, T., Hrabe de Angelis, I., Araújo, A., et al. (2016). Longterm observations of cloud condensation nuclei in the Amazon rain forest – Part 1: Aerosol size distribution, hygroscopicity, and new model parametrizations for CCN prediction. *Atmospheric Chemistry and Physics*, *16*(24), 15709–15740. https://doi.org/10.5194/acp-1615709-2016

Romps, D. M., Seeley, J. T., Vollaro, D., & Molinari, J. (2014). Projected increase in lightning strikes in the United States due to global warming. *Science*, *346*(6211), 851–854. https://doi.org/10.1126/science.1259100

Rycroft, M. J., Nicoll, K. A., Aplin, K. L., & Harrison, R. G. (2012). Recent advances in global electric circuit coupling between the space environment and the troposphere. *Journal of Atmospheric and Solar-Terrestrial Physics*, *90*(91), 198–211. https://doi.org/10.1016/j.jastp.2012.03.015

Sahu, L. K., & Lal, S. (2006). Changes in surface ozone levels due to convective downdrafts over the Bay of Bengal. *Geophysical Research Letters*, *33*(10), L10807. https://doi.org/10.1029/2006GL025994

Scala, J. R., Garstang, M., Tao, W.-K., Pickering, K. E., Thompson, A. M., Simpson, J., et al. (1990). Cloud draft structure and trace gas transport. *Journal of Geophysical Research*, *95*(D10), 17015–17030. https://doi.org/10.1029/JD095iD10p17015

Schumann, U., & Huntrieser, H. (2007). The global lightning-induced nitrogen oxides source. *Atmospheric Chemistry and Physics*, *7*(14), 3823–3907. https://doi.org/10.5194/acp-7-3823-2007

Seeley, J. T., & Romps, D. M. (2015). The effect of global warming on severe thunderstorms in the United States. *Journal of Climate*, *28*(6), 2443–2458. https://doi.org/10.1175/JCLI-D-14-00382.1

Sinha, A., & Toumi, R. (1997). Tropospheric ozone, lightning, and climate change. *Journal of Geophysical Research*, *102*(D9), 10667–10672. https://doi.org/10.1029/96JD03710

Ståhle, L., & Wold, S. (1989). Analysis of Variance (ANOVA). *Chemometrics and Intelligent Laboratory Systems*, *6*(4), 259–272. https://doi.org/10.1016/0169-7439(89)80095-4

Tibshirani, R. (1996). Regression shrinkage and selection via the lasso. *Journal of the Royal Statistical Society: Series B*, *58*(1), 267–288. https://doi.org/10.1111/j.2517-6161.1996.tb02080.x

Toumi, R., Haigh, J. D., & Law, K. S. (1996). A tropospheric ozone-lightning climate feedback. *Geophysical Research Letters*, *23*(9), 1037–1040. https://doi.org/10.1029/96GL00944

Tridon, F., Battaglia, A., Kollias, P., Luke, E., & Williams, C. R. (2013). Signal postprocessing and reflectivity calibration of the atmospheric radiation measurement program 915-MHz wind profilers. *Journal of Atmospheric and Oceanic Technology*, *30*(6), 1038–1054. https://doi.org/10.1175/JTECH-D-12-00146.1

Twomey, S. (1956). The electrification of individual cloud droplets. *Tellus*, *8*(4), 445–452. https://doi.org/10.1111/j.2153-3490.1956.tb01247.x

Unfer, G. R., Machado, L. A. T., Albrecht, R., Cecchini, M., Harder, H., Magina, F. C., et al. (2023). Dataset: "Decoding the relationship between cloud electrification, downdrafts, and surface ozone in the Amazon Basin" (version 3) [Dataset]. *Zenodo*. https://doi.org/10.17617/3.5S5XUV

Verma, S., Yadava, P. K., Lal, D. M., Mall, R. K., Kumar, H., & Payra, S. (2021). Role of lightning NOx in ozone formation: A review. *Pure and Applied Geophysics*, *178*(4), 1425–1443. https://doi.org/10.1007/s00024-021-02710-5

Wennberg, P. O., Bates, K. H., Crounse, J. D., Dodson, L. G., McVay, R. C., Mertens, L. A., et al. (2018). Gas-Phase reactions of isoprene and its major oxidation products. *Chemical Reviews*, *118*(7), 3337–3390. https://doi.org/10.1021/acs.chemrev.7b00439

White, A. B., Mahoney, K. M., Cifelli, R., & King, C. W. (2015). Wind profilers to aid with monitoring and forecasting of high-impact weather in the southeastern and western United States. *Bulletin of the American Meteorological Society*, *96*(12), 2039–2043. https://doi.org/10.1175/BAMS-D-14-00170.1

Williams, E., Rosenfeld, D., Madden, N., Gerlach, J., Gears, N., Atkinson, L., et al. (2002). Contrasting convective regimes over the Amazon. *Journal of Geophysical Research*, *107*(D20), 8082. https://doi.org/10.1029/2001JD000380

Zeng, G., Pyle, J. A., & Young, P. J. (2008). Impact of climate change on tropospheric ozone and its global budgets. *Atmospheric Chemistry and Physics*, *8*(2), 369–387. https://doi.org/10.5194/acp-8-369-2008